11-2008

Kinetic and Spectroscopic Analysis of the Catalytic Role of H79 in the Methionine Aminopeptidase from *Escherichia coli*

Sarah J. Watterson
Utah State University

Sanghamitra Mitra
Utah State University

Sabina I. Swierczek
Utah State University

Brian Bennett
Marquette University, brian.bennett@marquette.edu

Richard C. Holz
Marquette University, richard.holz@marquette.edu

Biochemistry, Vol. 47, No. 45 (11 November 2008): 11885–11893. DOI.

Kinetic and Spectroscopic Analysis of the Catalytic Role of H79 in the Methionine Aminopeptidase from *Escherichia coli*

Sarah J. Watterson
Department of Chemistry and Biochemistry, Utah State University, Logan, Utah
Sanghamitra Mitra
Department of Chemistry and Biochemistry, Utah State University, Logan, Utah
Sabina I. Swierczek
Department of Chemistry and Biochemistry, Utah State University, Logan, Utah
Brian Bennett
National Biomedical EPR Center, Department of Biophysics, Medical College of Wisconsin, Milwaukee, Wisconsin
Richard C. Holz
Department of Chemistry and Biochemistry, Utah State University, Logan, Utah
Department of Chemistry, Loyola University, Chicago, Illinois

SUBJECTS:

Peptides and proteins, Metals, Isotope effects, Ions

Abstract

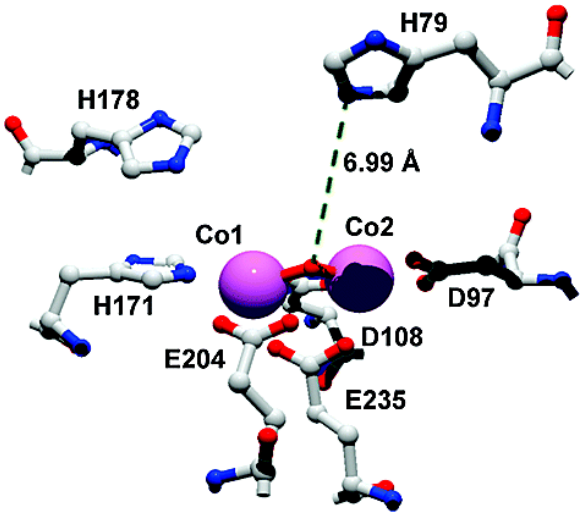

To gain insight into the role of the strictly conserved histidine residue, H79, in the reaction mechanism of the methionyl aminopeptidase from *Escherichia coli* (*Ec*MetAP-I), the H79A mutated enzyme was prepared. Co(II)-loaded H79A exhibits an overall >7000-fold decrease in specific activity. The almost complete loss of activity is primarily due to a >6000-fold decrease in k_{cat}. Interestingly, the K_m value obtained for Co(II)-loaded H79A was approximately half the value observed for wild-type (WT) *Ec*MetAP-I. Consequently, k_{cat}/K_m values decreased only 3000-fold. On the other hand, the observed specific activity of Mn(II)-loaded H79A *Ec*MetAP-I decreased by ∼2.6-fold while k_{cat} decreased by ∼3.5-fold. The observed K_m value for Mn(II)-loaded H79A *Ec*MetAP-I was ∼1.4-fold larger than that observed for WT *Ec*MetAP-I, resulting in a k_{cat}/K_m value that is lower by ∼3.4-fold. Metal binding, UV−vis, and EPR data indicate that the active site is unperturbed by mutation of H79, as suggested by X-ray crystallographic data. Kinetic isotope data indicate that H79 does not transfer a proton to the newly forming amine since a single proton is transferred in the transition state for both the WT and H79A *Ec*MetAP-I enzymes. Therefore, H79 functions to position the substrate by hydrogen bonding to either the amine group of the peptide linkage or a backbone carbonyl group. Together, these data provide new insight into the catalytic mechanism of *Ec*MetAP-I.

Methionine aminopeptidases (MetAPs) are ubiquitous enzymes responsible for the cleavage of N-terminal methionine residues from polypeptide chains (2-5). Methionine is the universal initiator of protein synthesis, and the removal of methionine is critical in protein maturation processes (6, 7). The physiological importance of MetAP activity is underscored by the cellular lethality upon deletion of MetAP genes in *Escherichia coli*, *Salmonella typhimurium*, and *Saccharomyces cerevisiae*(8-11). Moreover, a MetAP from eukaryotes has been identified as the molecular target for the antiangiogenesis drugs ovalicin and fumagillin, among others (12-16). Therefore, the inhibition of MetAP activity in tumors is an emerging therapy for the prevention of tumor vascularization, which often leads to tumor regression due to oxygen and nutrient deprivation. Used in conjunction with standard cancer therapies, including surgery, radiation, and/or chemotherapy, antiangiogenic drugs are used to shrink localized tumors and protect against metastasis. Targeting angiogenesis for cancer treatment has a number of advantages, including low cellular toxicity and a lack of drug resistance (15), since it is a disease-specific therapy.

MetAPs are organized into two classes (types I and II) on the basis of the absence or presence of an extra 62-amino acid sequence (of unknown function) inserted near the catalytic domain of type II enzymes. The type I MetAPs from *E. coli* (*Ec*MetAP-I),1*Staphylococcus aureus* (*Sa*MetAP-I), *Thermotoga maritima* (*Tm*MetAP-I), and *Homo sapiens* (*Hs*MetAP-I) and the type II MetAPs from *H. sapiens* (*Hs*MetAP-II) and *Pyrococcus furiosus* (*Pf*MetAP-II) have been crystallographically characterized (15, 17-22). All six display a novel "pita-bread" fold with an internal pseudo-2-fold symmetry that structurally relates the first and second halves of the polypeptide chain to each other. Each half contains an antiparallel β-pleated sheet that is flanked by two α-helical segments. Both domains contribute conserved residues as ligands to the divalent metal ions residing in the active site. In addition, all six structures contain a bis(μ-carboxylato)(μ-aquo/hydroxo)dicobalt(II) core with an additional carboxylate residue at each metal site and a single histidine bound to Co1 (Figure 1) (23, 24). Recently, an X-ray crystal structure of *Ec*MetAP-I was reported with only a single Mn(II) ion bound in the active site (25). This structure was obtained by limiting the amount of metal ion present during crystal growth. The beauty of this structure is that it provides the first structural verification that MetAPs can form mononuclear active sites and are fully active, and the single divalent metal ion resides on the H171 side of the active site as previously predicted by ^{1}H NMR and EXAFS spectroscopy (23, 24).

Abbreviations: *Ec*MetAP-I, methionine aminopeptidase from *E. coli*; *Pf*MetAP-II, methionine aminopeptidase from *P. furiosus*; HEPES, 4-(2-hydroxyethyl)-1-piperazineethanesulfonic acid; ICP-AES, inductively coupled plasma atomic emission spectroscopy.

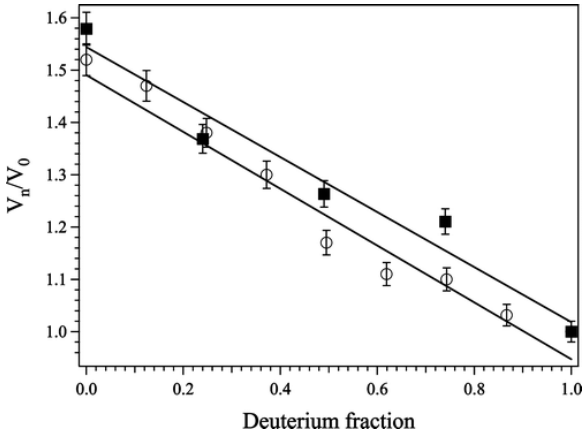

Figure 1. Plot of V_n/V_0 vs atom fraction of deuterium for WT (■) and H79A (◯) *Ec*MetAP-I at pH 7.5. V_n/V_0 is defined as the velocity at *n* atom fraction of deuterium over the velocity in water. Each point is an average of three replicates.

The catalytic roles of both the active site metal ions as well as active site residues have been proposed (1, 25-27). However, the proposed catalytic mechanism for MetAP assigns no definitive role to the conserved histidine (H79; *E. coli* numbering), which resides ∼8 Å from the first metal binding site (26). On the basis of X-ray crystallographic data for both type I and II MetAPs bound by several substrate, transition state, and product inhibitors as well as fumagillin, H79 has been thought to help position the substrate in the active site and/or to transfer a proton to the newly formed N-terminal amine (15, 28). A significant aspect of designing small molecules that specifically target MetAPs requires a detailed understanding of how potential antiangiogenic inhibitors interact with MetAPs. To determine the catalytic role of H79, we have prepared the H79A mutant *Ec*MetAP-I and characterized the enzyme using kinetic and spectroscopic methods.

Materials and Methods

Mutagenesis, Protein Expression, and Purification

All chemicals used in this study were purchased commercially and were of the highest quality available. The H79A-altered *Ec*MetAP-I enzyme was generated as previously reported (16). Recombinant WT and H79A *Ec*MetAP-I were expressed and purified as previously described (29, 30). Purified H79A *Ec*MetAP-I exhibited a single band on SDS−PAGE, indicating an overall purity of >95%. Protein concentrations were estimated from the absorbance at 280 nm using an extinction coefficient of 16450 M^{-1} cm^{-1}. Apo-*Ec*MetAP-I H79A samples were exchanged into 25 mM HEPES (pH 7.5) containing 150 mM KCl (Centricon-10, Millipore Corp.). Samples were stored frozen at −80 °C until they were needed.

Metal Content Measurement

The concentrations of H79A and WT *Ec*MetAP-I samples used for metal analysis were typically 30 μM. Apo-*Ec*MetAP-I samples were incubated under anaerobic conditions with MCl_2, where M is Co(II) or Fe(II) (MCl_2, 99.999%, Strem Chemicals, Newburyport, MA, or Aldrich, St. Louis, MO), for 30 min prior to exhaustive dialysis under anaerobic conditions against Chelex-100-treated buffer as previously reported (29, 30). Analyses were performed using inductively coupled plasma atomic emission spectrometry (ICP-AES).

Enzymatic Assay of H79A *Ec*MetAP-I

H79A *Ec*MetAP-I was assayed for catalytic activity using the tetrapeptide MGMM as the substrate (8 mM) with a high-performance liquid chromatography (HPLC) assay as previously described with minor modifications (30). The reaction mixture consisted of a 4 μL aliquot of a 100 μM enzyme solution and 3 equiv of a metal solution. Various concentrations of substrate were added to the enzyme solution to a final volume of 20 μL [25 mM HEPES in Chelex-100-treated water (pH 7.5) containing 150 mM KCl]. The reaction time was 24 h. This method is based on the spectrophotometric quantitation of the reaction product tripeptide, GMM, following separation on a C8 HPLC column (Phenomenex, Luna; 5, 4.6 Å ∼ 25 cm). The kinetic parameter *v* (velocity) was determined at pH 7.5 by quantifying the tripeptide GMM at 215 nm in triplicate. One unit of activity is defined as the amount of enzyme that produces 1 μmol of GMM/min. The metal binding titration reaction was carried out using the same conditions with titrated metal concentrations of up to 10 equiv using either Co(II) or Mn(II).

Isothermal Titration Calorimetry

Isothermal titration calorimetry (ITC) measurements were conducted using a MicroCal OMEGA ultrasensitive titration calorimeter. The titrant ($CoCl_2$) and apo-WT and H79A *Ec*MetAP-I solutions were prepared in Chelex-100-treated 25 mM HEPES buffer (pH 7.5) containing 150 mM KCl. Stock buffer solutions were thoroughly degassed before each titration. The enzyme solution (70 μM) was placed in the calorimeter cell and stirred at 200 rpm to ensure rapid mixing. Typically, 3 μL of titrant was delivered over 7.6 s with a 5 min interval between injections to allow for complete equilibration. Each titration was continued until 4.5−6 equiv of Co(II) had been added to ensure that no additional complexes were formed in excess titrant. A background titration, consisting of the identical titrant solution but only the buffer solution in the sample cell, was subtracted from each experimental titration to account for the heat of dilution. These data were analyzed with a two- or three-site binding model using the Windows-based Origin software package supplied by MicroCal.

Spectroscopic Measurements

Electronic absorption spectra were recorded using a Shimadzu UV-3101PC spectrophotometer. All apo-*Ec*MetAP-I samples used in spectroscopic measurements were thoroughly degassed prior to incubation with Co(II) ($CoCl_2$) for ∼20 min at 25 °C. Co(II)-containing samples were handled throughout in an anaerobic glovebox (N_2/5% H_2, 1 ppm O_2; Coy Laboratories). Electronic absorption spectra were normalized for protein concentration and the absorption due to uncomplexed Co(II) (512 nm = 6.0 M^{-1} cm^{-1}). Low-temperature EPR

spectroscopy was performed using a Bruker ESP-300E spectrometer equipped with an ER 4116 DM dual-mode X-band cavity and an Oxford Instruments ESR-900 helium flow cryostat.

Solvent Isotope Effect

All buffers were prepared from a freshly opened bottle of 99.9% [^{2}H]H_2O (Aldrich). The buffers and Co(II) salts used in the preparation of all deuterated buffers were in the anhydrous form. The pHs of all the buffers used were adjusted via addition of NaOD or DCl [both at 99% deuterium content (Acros Organics, Geel, Belgium)] and corrected for deuteration by adding 0.4 to the reading of the pH electrode ($p^2H = p^1H$ meter reading + 0.4) (31). The kinetic assay was performed as previously described with the exception of the replacement of H_2O with D_2O.

Results

Metal Content and Specific Activity of H79A *Ec*MetAP-I

The number of tightly bound divalent metal ions was determined for H79A *Ec*MetAP-I by ICP-AES. Apoenzyme samples (30 μM), to which 2−30 equiv of Co(II) had been added under anaerobic conditions, were dialyzed for 3 h at 4 °C with Chelex-100-treated, metal-free HEPES buffer [25 mM HEPES and 150 mM KCl (pH 7.5)]. ICP-AES revealed 1.0 ± 0.1 equiv of cobalt-associated H79A-altered *Ec*MetAP-I, similar to the amount of WT *Ec*MetAP-I (23).

The specific activity of H79A *Ec*MetAP-I was determined with the tetrapeptide substrate MGMM. Since the H79A enzyme was stored as the apo form, it was preincubated with 3 equiv of Co(II) for ∼30 min prior to all kinetic experiments. The apo form of H79A *Ec*MetAP-I was catalytically inactive. Kinetic parameters were determined for Co(II)- and Mn(II)-loaded H79A and WT *Ec*MetAP-I (Table 1). Co(II)-loaded H79A exhibits an overall >7000-fold decrease in specific activity. The almost complete loss of activity is primarily due to a >6000-fold decrease in k_{cat}. Interestingly, the K_m value obtained for Co(II)-loaded H79A was approximately half the value observed for WT *Ec*MetAP-I. Consequently, k_{cat}/K_m values decreased only 3000-fold. Kinetic parameters were also determined for Mn(II)-loaded H79A and WT *Ec*MetAP-I (Table 1). For Mn(II)-loaded H79A *Ec*MetAP-I, the specific activity decreased by ∼2.6-fold while k_{cat} decreased by ∼3.5-fold. The observed K_m value for Mn(II)-loaded H79A *Ec*MetAP-I was only ∼1.4 times larger than that observed for WT *Ec*MetAP-I, resulting in a k_{cat}/K_m value that is lower by only ∼3.4-fold.

Table 1. Kinetic Parameters for H79A *Ec*MetAP-I toward MGMM in the Presence of 3 equiv of Mn(II) or Co(II) at pH 7.5

metal ion	kinetic parameter	wild type	H79A
Co(II)	K_m (mM)	3.2 ± 0.1	1.5 ± 0.1
	k_{cat} (s^{-1})	18.3 ± 0.1	0.003 ± 0.001
	k_{cat}/K_m (M^{-1} s^{-1})	5720	2
Mn(II)	K_m (mM)	1.3 ± 0.2	1.8 ± 0.1
	k_{cat} (s^{-1})	4.6 ± 0.1	1.8 ± 0.1
	k_{cat}/K_m (M^{-1} s^{-1})	3500	1000

Solvent Isotope Effect

The solvent isotope effect was determined for both WT and H79A *Ec*MetAP-I using MGMM as the substrate at pH 7.6. k_{cat} values for MGMM were measured at several ratios of D_2O and H_2O, and the results were plotted as the atom fraction of deuterium versus V_n/V_0, where V_n is the observed velocity at n fraction of deuterium and V_0 is the observed velocity in water (Figure 1). Proton inventories were obtained by fitting the experimental data to equations derived from the Gross-Butler equation (eq 1):

$$V_n/V_0 = \frac{\prod_i^{v_T}(1 - n + n\varphi_i^T)}{\prod_i^{v_T}(1 - n + n\varphi_j^R)}$$

(1)

where n is the atom fraction of deuterium, V_n and V_0 are the same as described above, v_T is the number of protons transferred in the transition state, v_R is the number of protons transferred in the reactant state, and φ is the fractionation factor defined as

$$\varphi = \left(X_i^D/X_i^H\right)/[n/(1-n)]$$

(2)

where X_i^D and X_i^H are the mole fractions of deuterons and protons in the ith transition or reactant state, respectively, while the subscripts T and R refer to the transition and reactant state, respectively (32, 33). At pH 7.6, the best fit for both WT and H79A *Ec*MetAP-I exhibited linearity, suggesting that one proton is transferred in the transition state of the catalytic reaction (Figure 1). The fit yielded fractionation factors of 0.80 and 0.79 for WT and H79A *Ec*MetAP-I, respectively.

Since the largest deviations for theoretical proton inventory curves occur at atom fractions of 0.5 (34, 35), calculation of the midpoint partial solvent isotope effect can provide insight into the number of protons involved in the catalytic reaction. The following equations, derived by Elrod (34), allowed for the calculation of midpoint partial solvent isotope effects when the experimental data were obtained at different atom fractions:

$$\text{one protons } V_m / V_1) = (1 - n_m)(V_0 / V_1) + n_m$$

(3)

$$\text{two protons } (V_m/V_1) = [(1 - n_m)(V_0 / V_1)^{1/2} + n_m]^2$$

(4)

$$\text{general solvation } (V_m/V_1) = (V_0 / V_1)^{(1 - n_m)}$$

(5)

where n_m = 0.49 (the H_2O/D_2O ratio at the midpoint), V_m/V_1 equals the midpoint partial solvent isotope effect, and V_0/V_1 represents the total isotope effect (velocity in 100% H_2O/velocity in 100% D_2O). The experimental and calculated midpoint partial isotope effects are presented in Table 2. At pH 7.6, comparison of the theoretical and experimental midpoint partial isotope effects for both WT and H79 *Ec*MetAP-I suggests that one proton is transferred at this pH. However, the midpoint partial solvent isotope effect calculations could not strongly distinguish between one proton transfer and general solvation effects (Table 2).

Table 2. Midpoint Solvent Isotope Effect Data for WT and H79A *Ec*MetAP-I Using MGMM as the Substratea

			calculated midpoint solvent isotope effect		
enzyme	**V_0/V_1**	**midpoint solvent isotope effect (V_m/V_1)**	**one proton**	**two protons**	**general solvation**
WT	1.6	1.26	1.27	1.28	1.25

H79A	1.5	1.17	1.21	1.24	1.22

[a]Experimental and theoretical midpoint isotope effects were calculated for a 0.49 atom fraction of deuterium.

Metal Binding Properties of H79A *Ec*MetAP-I

To examine the metal binding properties of the H79A *Ec*MetAP-I enzyme, we titrated Mn(II) and Co(II) into apo-H79A *Ec*MetAP-I (Figure 2). The dissociation constant (K_d) for the first divalent metal binding event for both Mn(II) and Co(II) was obtained by fitting these titration data to eq 6(36):

$$r = pC_s / (K_d + C_s)$$

(6)

where p is the number of sites for which interaction with M(II) is governed by the intrinsic dissociation constant K_d and r is the binding function calculated by conversion of the fractional saturation (f_a) using eq 7 as previously described (23).

$$r = f_a p$$

(7)

C_s, the free metal concentration, was calculated using eq 8

$$C_s = C_{TS} - rC_A$$

(8)

where C_{TS} and C_A are the total molar concentrations of metal and enzyme, respectively. K_d values were obtained for both Mn(II) and Co(II) by fitting these data via an iterative process that allowed both K_d and p to vary (Figure 2). The best fits obtained provided p values of ~1 and K_d values of 0.4 ± 0.1 and 0.5 ± 0.1 μM for Mn(II) and Co(II) binding, respectively.

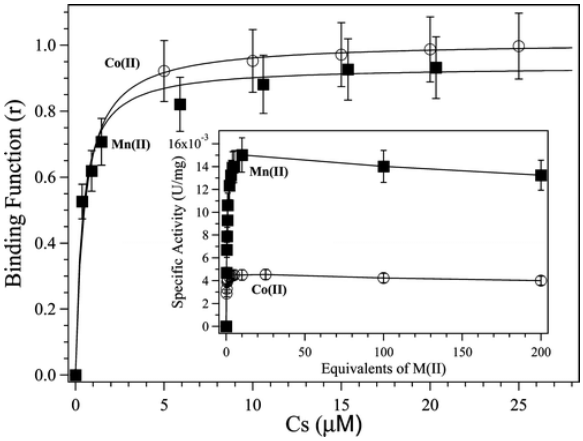

Figure 2. Plot of binding function r vs C_s (the free metal ion concentration) for Co(II) and Mn(II) binding to H79A *Ec*MetAP-I. The solid lines represent the theoretical fit to the data using eq 1. These fits provide a p value of ~1 and K_d values of 0.5 ± 0.1 and 0.4 ± 0.1 μM for Co(II) and Mn(II), respectively. The inset shows a plot of specific activity (units per milligram) vs equivalents of Co(II) and Mn(II). All activity assays were conducted using 8 mM MGMM in 25 mM HEPES (pH 7.5) and 150 mM KCl.

In addition, isothermal titration calorimetry (ITC) was employed to determine the association constants (K_a) for both Co(II) and Mn(II) binding to H79A *Ec*MetAP-I at 25.0 ± 0.2 °C (Figure 3). K_a values were obtained by fitting the ITC data, after subtraction of the background heat of dilution, via an iterative process using Origin. This software package uses a nonlinear least-squares algorithm that allows the concentrations of the titrant and the sample to be fit to the heat flow per injection to an equilibrium binding equation for two sets of noninteracting sites. The K_a value, the metal/enzyme stoichiometry (n), and the change in enthalpy ($\Delta H°$) were allowed to vary during the fitting process (Table 3 and Figure 3). The relationship between K_a and the dissociation constant is defined as

$$K_d = 1 / K_a$$

(9)

The best fits obtained for H79A *Ec*MetAP-I provided an overall n value of 3, indicating three noninteracting sites. Attempts to fit these data with n values of 1 or 2 provided poor fits. For Co(II) and Mn(II) binding to H79A *Ec*MetAP-I, the observed K_d values for the first binding event are 1.4 ± 1.5 and 5.3 ± 1.4 µM, respectively, which are within error of those observed for WT *Ec*MetAP-I. The second and third metal binding events are equivalent for H79A *Ec*MetAP-I and provided K_d values of 1.6 ± 0.8 and 0.08 ± 0.02 mM for Co(II) and Mn(II), respectively.

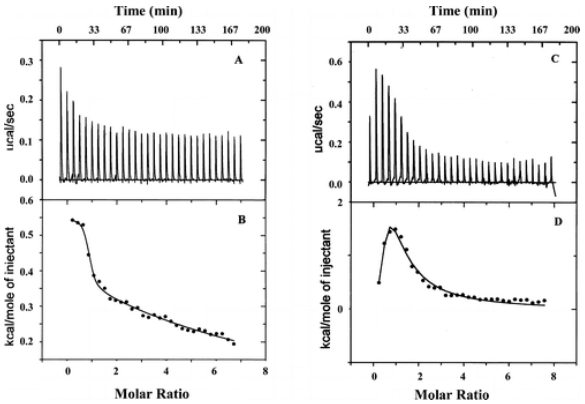

Figure 3. Isothermal titration calorimetry (ITC) titrations of 70 µM solutions of H79A *Ec*MetAP-I with 5 mM Co(II) (A) or 5 mM Mn(II) (C). The best fits of the data in panels A and C are shown in panels B and D, respectively, after subtraction of the heat of dilution.

Table 3. ITC Data for the Mn(II)- and Co(II)-Loaded H79A *Ec*MetAP-I Enzymes

	*n*a	K_{a1}, K_{a2} (M^{-1})	K_{d1}, K_{d2} (μM)	ΔH°_1, ΔH°_2 (kcal/mol)	$T\Delta S^\circ_1$, $T\Delta S^\circ_2$ (kcal/mol)	ΔG°_1, ΔG°_2 (kcal/mol)
[CoCo(*Ec*MetAP-I)]	1	6.36×10^5	1.6	15700	15708	−7.8
	2	7.05×10^1	14200	1.1×10^6	1.1×10^6	−2.5
[MnMn(*Ec*MetAP-I)]	2	3.31×10^5	3.0	2600	2607	−7.4
	1	2.27×10^2	4400	33800	33803	−3.2
[CoCo(H79A)]	1	7.35×10^5	1.4	549	557	−7.9
	2	6.41×10^2	1600	9770	9774	−3.8
[MnMn(H79A)]	1	1.90×10^5	5.3	−461	−454	−7.1
	2	1.34×10^4	80	20900	20905	−5.5

[a]All fits were performed using an *n* value of 3, providing two distinct binding events with individual *n* values of 1 and 2.

The heat of reaction, measured during the ITC experiment, was converted into other thermodynamic parameters using the Gibbs free energy relationship:

$$\Delta G^\circ = -RT \ln(K_a) = \Delta H^\circ - T\Delta S^\circ$$

(10)

The thermodynamic parameters obtained for titrations of Co(II) and Mn(II) into WT and H79A *Ec*MetAP-I reveal changes that affect both of the metal binding sites (Table 3). Substitution of H79 with A makes the process of binding of the metal ions, particularly for the second metal ion, more spontaneous based on the more negative Gibbs free energies (Δ*G*).

UV−Vis Spectra of Co(II)-Loaded H79A

The electron absorption spectrum of H79A *Ec*MetAP-I was recorded as a function of Co(II) concentration and compared to that of WT *Ec*MetAP-I (Figure 4). For H79A *Ec*MetAP-I, the addition of 1 equiv of Co(II) produced maxima at 520 nm (ε = 58 M^{-1} cm^{-1}), 560 nm (ε = 72 M^{-1} cm^{-1}), and 620 nm (ε = 34 M^{-1} cm^{-1}). These absorption maxima are blue-shifted by ∼75 nm relative to those observed for WT *Ec*MetAP-I. Upon addition of a second equivalent of Co(II) to H79A *Ec*MetAP-I, the relative energies of all three observed maxima remained relatively constant; however, the molar absorptivities increased for each absorption band [520 nm (ε = 109 M^{-1} cm^{-1}), 560 nm (ε = 124 M^{-1} cm^{-1}), and 620 nm (ε = 66 M^{-1} cm^{-1})]. The observed increase is consistent with both metal ions residing in five-coordinate environments (24).

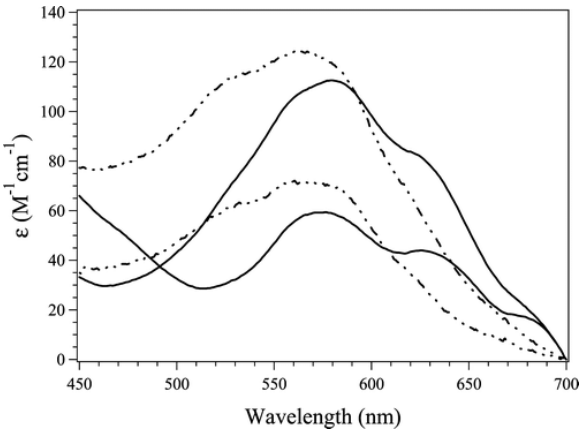

Figure 4. UV−vis spectra of H79A (−−−−) and WT (—) *Ec*MetAP-I in the presence of 1 and 2 equiv of Co(II). All spectra were recorded in 25 mM HEPES (pH 7.5) and 150 mM KCl.

EPR Spectra of Co(II)- and Mn(II)-Loaded H79A

The EPR spectrum of H79A *Ec*MetAP-I to which 1 equiv of Co(II) was added {"[Co_(H79A *Ec*MetAP-I)]"} provided an $S = {}^3/_2$ species, with only the $M_S = |\pm 1/2\rangle$ doublet populated from 6 to 60 K, and an essentially axial zero-field splitting (Figure 5A). The signal was very similar to, though distinguishable from, that of [Co_(WT *Ec*MetAP-I)] (Figure 5C). Both *Ec*MetAP-I signals displayed Curie law temperature dependence from 10 to 60 K. The observed EPR spectrum for [CoCo(H79A *Ec*MetAP-I)] (Figure 5B) was indistinguishable from that of [Co_(H79A *Ec*MetAP-I)] and also exhibited Curie law temperature dependence. This behavior mimicked that of the wild-type enzyme; the spectrum of [CoCo(WT *Ec*MetAP-I)] and its temperature dependence were indistinguishable from those of [Co_(WT *Ec*MetAP-I)]. Each of the spectra of Co(II) in the various forms of *Ec*MetAP-I exhibited microwave power-dependent rapid passage effects below 10 K; comparison of the extent to which the finishing baseline of the first integral of spectra recorded at 8 K overshot the starting baseline indicated that the susceptibility to

rapid passage effects was very similar for each of the species and that their relaxation properties were all, therefore, similar.

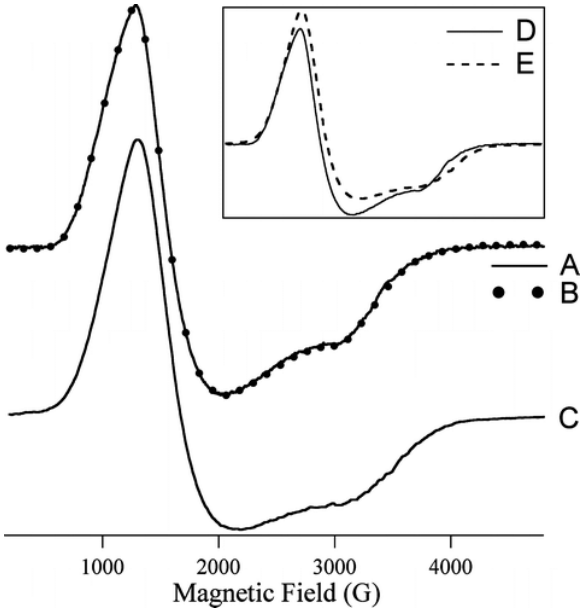

Figure 5. X-Band EPR spectra of Co(II)-substituted forms of *Ec*MetAP-I: (A) [Co_(H79A *Ec*MetAPI)], (B) [CoCo(H79A *Ec*MetAP-I)], and (C) [CoCo(WT *Ec*MetAP-I)]. Spectra A and B were recorded at 8 K with a 0.2 mW microwave power; spectrum C was recorded at 9 K with a 0.2 mW microwave power. The amplitude of trace A is shown multiplied by 1.88 compared to spectrum B. The inset shows the spectra of [CoCo(H79A *Ec*MetAP-I)] (D) and [CoCo(WT *Ec*MetAP-I)] (E) overlaid. All the spectra were recorded at a field modulation amplitude of 1.2 mT, a modulation frequency of 100 kHz, and a sweep rate of 10.2 mT s^{-1}, and the samples were in 25 mM HEPES buffer and 150 mM KCl (pH 7.5).

The EPR spectra of [Mn_(H79A *Ec*MetAP-I)] (Figure 6A,E) and [MnMn(H79A *Ec*MetAP-I)] (Figure 6B,F) were indistinguishable from each other but were subtly different from the mutually indistinguishable spectra of [Mn_(WT *Ec*MetAP-I)] (Figure 6C,G) and [MnMn(WT *Ec*MetAP-I)] (Figure 6D,H). Close examination of the spectra (e.g., the expanded regions of Figure 6A) revealed no evidence of an ∼45 G (4.5 mT) pattern due to inter-Mn(II) spin coupling. In addition, spectra from both WT and H79A *Ec*MetAP-I exhibited Curie law temperature dependence over a wide temperature range, and in contrast to WT *Ec*MetAP-I, no additional transitions were observed when the temperature was increased to 60 K. The Mn(II) signals from WT *Ec*MetAP-I were noticeably susceptible to rapid passage effects at low temperatures (6−8 K), while those of H79A *Ec*MetAP-I were not, indicating somewhat different relaxation properties.

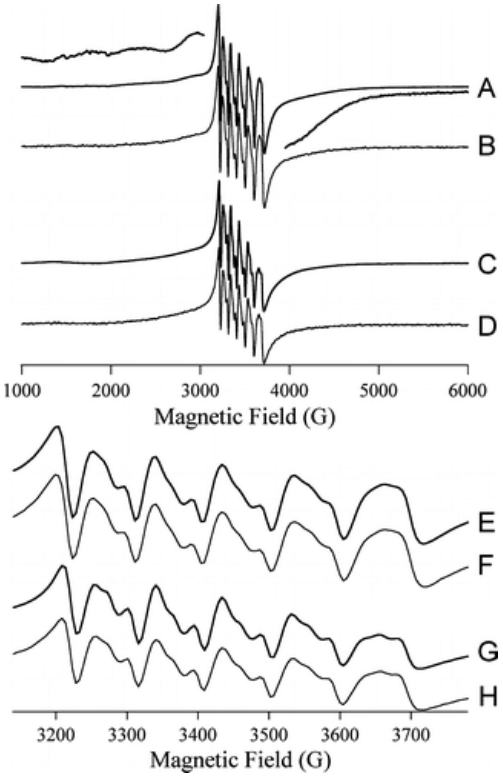

Figure 6. X-Band EPR spectra of Mn(II)-substituted forms of *Ec*MetAP-I: (A) [Mn_(H79A *Ec*MetAP-I)], (B) [MnMn(H79A *Ec*MetAP-I)], (C) [Mn_(WT *Ec*MetAP-I)], and (D) [MnMn(WT *Ec*MetAP-I)]. The high- and low-field wings of the spectrum of [Mn_(H79A *Ec*MetAP-I)] are shown with a larger (5 times) amplitude, above and below, respectively, trace A. Traces E−H are of the $g_{eff} \sim 2$ regions of spectra A−D, respectively. Spectra were recorded at 8 K with a microwave power of 0.2 mW, a field modulation amplitude of 1.2 mT, a modulation frequency of 100 kHz, and a sweep rate of 10.2 mT s^{-1}, and the samples were in 25 mM HEPES buffer and 150 mM KCl (pH 7).

Discussion

The active site histidine residues, H178 and H79, are strictly conserved in all MetAPs sequenced to date (6, 28). It has been suggested that both of these active site His residues play important roles in the catalytic removal of N-terminal methionine residues from polypeptide chains by MetAPs. While the catalytic role of H178 has been examined in some detail (1), the contributions of H79 to the hydrolysis reaction catalyzed by *Ec*MetAP-I remain unclear. Several catalytic functions have been prescribed to H79, some of which are (1, 6, 19, 28, 37) (i) proper positioning of the substrate, (ii) stabilizing the transition state through hydrogen bond formation, (iii) hydrogen bonding to the backbone amide of the scissile peptide bond, and (iv) acting as a general acid by providing a proton to the backbone amide of the scissile peptide bond forming the new N-terminal amine (1, 6). To investigate the role of H79 in catalysis, we have generated the H79A *Ec*MetAP-I enzyme and characterized this enzyme by kinetic and spectroscopic methods.

The specific activity of the H79A-altered *Ec*MetAP-I enzyme was determined in the presence of the tetrapeptide MGMM. Kinetic parameters for both Co(II)- and Mn(II)-loaded WT and H79A enzymes indicate that a significant amount of the observed effect on activity is due to a decrease in k_{cat}. The k_{cat} values for Co(II)- and Mn(II)-loaded H79A *Ec*MetAP-I decreased by ∼6100- and ∼2.6-fold, respectively. Interestingly, the observed K_m value for Co(II)-loaded H79A *Ec*MetAP-I decreased ∼2-fold compared to that of WT *Ec*MetAP-I; however, the observed K_m value for Mn(II)-loaded H79A *Ec*MetAP-I remained nearly identical to that of WT *Ec*MetAP-I. Consequently, the resulting catalytic efficiency (k_{cat}/K_m) for Co(II)- and Mn(II)-loaded H79A *Ec*MetAP-I decreased by ∼2900- and ∼3.5-fold, respectively. The more drastic loss of catalytic activity observed for the Co(II)-loaded

H79A enzyme compared to the Mn(II)-loaded H79A enzyme highlights the differences in the preferred coordination geometry (i.e., five- vs six-coordinate) for Co(II)- versus Mn(II)-loaded *Ec*MetAP-I enzymes. These data are also in line with previous studies on the Co(II)-loaded H79A-altered *Ec*MetAP-I enzyme (19, 28). They are also consistent with those reported for the Co(II)-loaded H231N *Hs*MetAP-II enzyme (H231 is equivalent to H79) in which a complete loss of activity was observed (37).

To determine the effects of altering H79 on the metal binding properties of *Ec*MetAP-I, the number of tightly bound metal ions and the K_d values for both metal binding sites were determined and compared to those of WT *Ec*MetAP-I. On the basis of ICP-AES analysis, ∼1.0 metal ion is tightly associated with the H79A *Ec*MetAP-I enzyme, as in WT *Ec*MetAP-I (23). Similarly, both the Co(II)- and Mn(II)-loaded H79A *Ec*MetAP-I enzymes exhibit K_d values identical, within error, to that of WT *Ec*MetAP-I. These data confirm that H79 is not directly involved in binding of the first divalent metal ion. For H79A and WT *Ec*MetAP-I, two additional weak metal binding events are also observed, the last of which is likely a remote Co(II) binding site identified in the X-ray crystal structure of *Ec*MetAP-I (16, 20). This remote metal binding site, or third metal binding site, was also observed in the structure of *Hs*MetAP-I (22). In both enzymes, this remote site is on the outer edge of the enzyme and becomes at least partially occupied at Co(II) concentrations near 1 mM. Interestingly, ITC data for the second Co(II) and Mn(II) binding events indicate that altering H79 to an Ala significantly increases the affinity of the second divalent metal ion binding site by factors of ∼10 and ∼25, respectively. The second β-sheet backbone of MetAP-I, which contains H79, also contains the active site ligands D108 and D97 which may perturb the metal ligating ability of those residues which are involved in binding the second divalent metal ion.

The observed electronic absorption and EPR spectra of H79A with 1 and 2 equiv of Co(II) are similar to those of WT *Ec*MetAP-I and are consistent with the X-ray crystal structure of H79A *Ec*MetAP-I, which suggests that both Co(II) ions are pentacoordinate (19). The slight blue shift observed in the electronic absorption spectrum of Co(II)-loaded H79A *Ec*MetAP-I versus WT *Ec*MetAP-I is possibly due to the perturbation of the β-sheet peptide backbone that contains the metal ligands D108 and D97. Although the differences between the electronic absorption and EPR spectra of WT and H79A *Ec*MetAP-I are slight, the very large difference in k_{cat} between these species suggests that the structural origins of these spectroscopic differences have catalytic relevance. The Co(II) concentration-normalized intensities of EPR spectra obtained for [Co_(H79A *Ec*MetAP-I)] and [CoCo(H79A *Ec*MetAP-I)] were indistinguishable. As with the EPR spectra, the d−d region of the electronic absorption spectrum of H79A *Ec*MetAP-I changed only in Co(II) concentration-dependent intensity upon addition of additional Co(II) to [Co_(H79A *Ec*MetAP-I)]. Entirely analogous behavior has been reported for WT *Ec*MetAP-I (23), and these data suggest that for both WT and H79A *Ec*MetAP, the natures and relative proportions of the Co(II) environments do not change upon addition of up to 2 equiv of Co(II).

Rationalization of these data with those obtained from ITC, kinetic, and X-ray crystallographic studies, at first, appears to be difficult. However, the most logical explanation leads to the conclusion that metal binding to MetAPs is cooperative and that discrepancies have arisen due to the concentrations of the enzyme samples used in the various experiments. For example, ITC data do not reveal cooperative binding of divalent metal ions to *Ec*MetAP-I or *Pf*MetAP-II but, instead, indicate that one metal ion binds with a much higher affinity than subsequent metal ions. It should be noted that ITC titrations are typically run with enzyme concentrations of ∼70 μM, and most often reveal two sets of binding sites (23). Likewise, initial activity assays carried out on *Ec*MetAP-I and *Pf*MetAP-II used enzyme concentrations of ∼20 μM, a value 2 orders of magnitude larger than the K_d value determined for the first metal binding site of 0.2 or 0.4 μM assuming a Hill coefficient of 1.3 or 2.1, respectively (38, 39). However, a K_d value between 2.5 and 4.0 μM was reported if it was assumed that only a single Co(II) binding site exists in the low-concentration regime, which is within error of ITC and kinetic K_d values. Spectroscopic and most X-ray crystallographic measurements were carried out at much higher enzyme (∼1 mM) and metal concentrations, where a significant concentration of dinuclear sites will undoubtedly be present.

Under the conditions utilized in ITC experiments, any cooperativity in divalent metal binding will not be detectable but may appear in EPR and electronic absorption data. Since activity titrations and ITC data are not particularly sensitive to the type of binding (i.e., cooperativity vs two independent binding sites), the weak cooperativity observed by Larrabee et al. (38) will not be observed in these experiments but is entirely consistent with the EPR and electronic absorption data and, indeed, with recent X-ray crystallographic data. Most X-ray structures of MetAPs were determined with a large excess of divalent metal ions, so only dinuclear sites are observed. However, crystallographic data obtained for *Ec*MetAP-I using metal ion:enzyme ratios of 0.5:1 reveal metal ion occupancies of 71% bound to the M1 site and 28% bound to the M2 site, consistent with cooperative binding (25).

While studies on the Co(II) form of MetAP may provide some mechanistic insight, Mn(II) or Fe(II) is more likely the physiological metal ion (29, 40, 41). EPR spectra obtained with 1 and 2 equiv of Mn(II) were indistinguishable (apart from intensity) and, similar to Co(II), suggest cooperativity in binding under the conditions that were employed. EPR spectra recorded on the Mn(II)-loaded H79A *Ec*MetAP-I enzyme suggested that the Mn(II) ions reside in a mixed oxygen/nitrogen coordination environment, as in the WT enzyme (42). However, in contrast to WT *Ec*MetAP-I and the type II MetAP from *P. furiosus*, no evidence of inter-Mn(II) spin coupling was observed for the Mn(II)-loaded H79A *Ec*MetAP-I enzyme from either parallel mode EPR, temperature dependence, or close examination of the spectra for a 45 G hyperfine pattern. In addition, the relaxation behaviors of Mn(II) in the WT and H79A enzymes differed. These data suggest subtle differences in the architecture of the dinuclear site in the WT versus H79A enzyme, possibly pertaining to a bridging ligand that, in WT *Ec*MetAP-I, mediates exchange coupling between the Mn(II) ions. That H79A *Ec*MetAP-I is only 2.5-fold less active than the WT enzyme suggests, in turn, that the putative bridging ligand is unimportant for activity and is, therefore, unlikely to be the source of the nucleophile.

A fundamental aspect of the catalytic mechanism of MetAPs that has not been addressed to date is the chemical identity of the rate-limiting step. Kinetic isotope effect studies are an excellent way of gaining an understanding of the nature of the rate-limiting step as well as probing the transition state of catalytic reactions (43). Primary isotope effects are observed if a bond to the labeled atom is made or broken during the reaction, whereas secondary isotope effects describe processes at other positions. Therefore, we examined the solvent isotope effect of WT and H79A *Ec*MetAP-I using MGMM as the substrate at pH 7.6 (31) by substituting hydrogen (^{1}H) with deuterium (^{2}H). The presence of D_2O lowers the catalytic activity of both WT and H79A *Ec*MetAP-I, resulting in solvent isotope effects of 1.6 and 1.5, respectively. This is similar to the solvent isotope effect observed for carboxypeptidase A (1.3) (44), the aminopeptidase from *Aeromonas proteolytica* (2.8) (45), and the β-lactamase from *Bacteriodes fragilis* (2.6) (46). These results are consistent with a proton being transferred in the rate-limiting step of the reaction. Since the fractionation factor (φ) is characteristic of a proton−oxygen bond (neutral oxygen, 0.8−1.2) with a conventional isotope effect equal to 1 (33), the φ value of 0.80 suggests that an O−H bond is broken in the rate-limiting step. Since the rate-limiting step in peptide hydrolysis has previously been shown to be product formation (47), this may represent the protonation of the leaving group by a proton obtained from the hydroxide that reorganizes to a carbonyl group in the transition state after attacking the scissile peptide bond leading to the collapse of the transition state (Figure 7). Both WT and H79A *Ec*MetAP-I exhibit similar solvent isotope effects, suggesting that H79 is not involved in the transfer of a proton during catalytic turnover. Therefore, its function is likely limited to stabilization of the transition state by hydrogen bonding which facilitates the formation of the leaving group. These data are consistent with the proposed catalytic mechanism for MetAP and indicate that proton transfer processes limit the catalytic reaction (Figure 7).

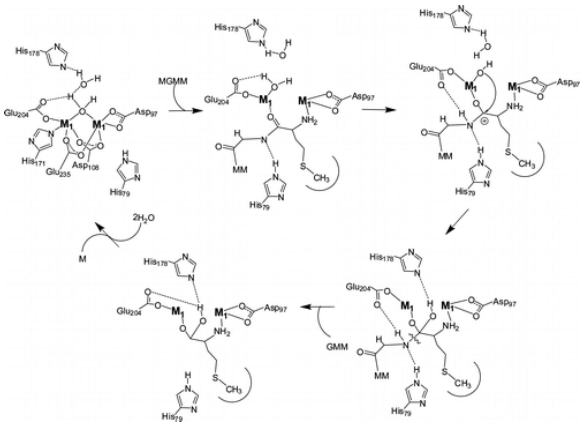

Figure 7. Proposed catalytic mechanism for MetAPs assuming cooperative metal binding.

In summary, several catalytic mechanisms for *Ec*MetAP-I have been proposed (19, 26) on the basis of kinetic, spectroscopic, X-ray crystallographic, and molecular modeling studies. In all of these mechanisms, donation of a proton by E204 or H79 to the leaving group amino nitrogen was proposed to cause the collapse of the transition state into the corresponding products. However, on the basis of data presented herein, H79 does not transfer a proton to the newly forming amine since a single proton is transferred in the transition state for both WT and H79A *Ec*MetAP-I (Figure 7). Therefore, H79 is not essential as a general acid during catalysis, which suggests that the single observed proton transfer is likely due to E204 transferring a proton to the peptide backbone amide. The starkly different effects of H79A substitution on the catalytic activities of Mn(II)- and Co(II)-containing *Ec*MetAP-I suggest that the role of H79 is dependent on some property of the metal ion that is not shared by Co(II) and Mn(II). Where Co(II) is five-coordinate in *Ec*MetAP-I, Mn(II) prefers six-coordinate geometries. A role for H79 in positioning the substrate, by hydrogen bonding to either the amine group of the peptide linkage or a backbone carbonyl group, would indeed cause the catalytic efficiency to be very sensitive to the geometry of the metal ion. Analogues of both of these putative interactions between H79 and substrate have been observed in X-ray crystallographic studies with inhibitors (6). This role is also consistent with the observed differences in activity for different length peptides as well as the observed difference in k_{cat} values for Co(II)- versus Mn(II)-loaded H79A enzymes.

References

1 Copik, A. J., Swierczek, S. I., Lowther, W. T., D'souza, V., Matthews, B. W., and Holz, R. C.**2003** Kinetic and Spectroscopic Characterization of the H178A Mutant of the Methionyl Aminopeptidase from *Escherichia coli* Biochemistry 42 6283 6292

2 Bradshaw, R. A.**1989** Protein translocation and turnover in eukaryotic cells Trends Biochem. Sci. 14 276 279

3 Meinnel, T., Mechulam, Y., and Blanquet, S.**1993** Methionine as Translation Start Signal: A Review of the Enzymes of the Pathway in *Escherichia coli* Biochimie 75 1061 1075

4 Bradshaw, R. A., Brickey, W. W., and Walker, K. W.**1998** N-terminal processing: The methionine aminopeptidase and N^{α}-acetyl transferase families Trends Biochem. Sci. 23 263 267

5 Arfin, S. M., and Bradshaw, R. A.**1988** Cotranslational processing and protein turnover in eukaryotic cells Biochemistry 2721 7979 7984

6 Lowther, W. T., and Matthews, B. W.**2002** Metalloaminopeptidases: Common Functional Themes in Disparate Structural Suroundings Chem. Rev. 102 4581 4607

7 Lowther, W. T., and Matthews, B. W.**2000** Structure and function of the methionine aminopeptidases Biochim. Biophys. Acta 1477 157 167

8 Chang, S.-Y. P., McGary, E. C., and Chang, S.**1989** Methionine Aminopeptidase gene of *Escherichia coli* is essential for cell growth J. Bacteriol. 1717 4071 4072

9 Chang, Y.-H., Teichert, U., and Smith, J. A.**1992** Molecular cloning, sequencing, deletion, and overexpression of a methionine aminopeptidase gene from *Saccharomyces cerevisiae* J. Biol. Chem. 267 8007 8011
10 Li, X., and Chang, Y.-H.**1995** Amino terminal protein processing in *Saccharomycescerevisiae* is an essential function that requires two distinct methionine aminopeptidases Proc. Natl. Acad. Sci. U.S.A. 92 12357 12361
11 Miller, C. G., Kukral, A. M., Miller, J. L., and Movva, N. R.**1989** *pepM* is an essential gene in *Salmonella typhimurium* J. Bacteriol. 171 5215 5217
12 Taunton, J.**1997** How to starve a tumor Chem. Biol. 4 493 496
13 Griffith, E. C., Su, Z., Turk, B. E., Chen, S., Chang, Y. H., Wu, Z., Biemann, K., and Liu, J. O.**1997** Methionine aminopeptidase (type 2) is the common target for angiogenesis inhibitors AGM-1470 and ovalicin Chem. Biol. 4 461 471
14 Sin, N., Meng, L., Wang, M. Q., Wen, J. J., Bornmann, W. G., and Crews, C. M.**1997** The anti-angiogenic agent fumagillin covalently binds and inhibits the mathionine aminopeptidase, MetAP-2 Proc. Natl. Acad. Sci. U.S.A. 94 6099 6103
15 Liu, S., Widom, J., Kemp, C. W., Crews, C. M., and Clardy, J.**1998** Structure of the human methionine aminopeptidase-2 complexed with fumagillin Science 282 1324 1327
16 Lowther, W. T., McMillen, D. A., Orville, A. M., and Matthews, B. W.**1998** The anti-angiogenic agent fumagillin covalently modifies a conserved active site histidine in the *Escherichia coli* methionine aminopeptidase Proc. Natl. Acad. Sci. U.S.A. 95 12153 12157
17 Douangamath, A., Dale, G. E., D'Arcy, A., Almstetter, M., Eckl, R., Frutos-Hoener, A., Henkel, B., Illgen, K., Nerdinger, S., Schulz, H., MacSweeney, A., Thormann, M., Treml, A., Pierau, S., Wadman, S., and Oefner, C.**2004** J. Med. Chem. 47 1325 1328
18 Tahirov, T. H., Oki, H., Tsukihara, T., Ogasahara, K., Yutani, K., Ogata, K., Izu, Y., Tsunasawa, S., and Kato, I.**1998** Crystal structure of the methionine aminopeptidase from the hyperthermophile *Pyrococcus furiosus* J. Mol. Biol. 284 101 124
19 Lowther, W. T., Orville, A. M., Madden, D. T., Lim, S., Rich, D. H., and Matthews, B. W.**1999** *Escherichia coli* Methionine Aminopeptidase: Implications of crystallographic analyses of the native, mutant and inhibited enzymes for the mechanism of catalysis Biochemistry 38 7678 7688
20 Roderick, L. S., and Matthews, B. W.**1993** Structure of the Cobalt-Dependent Methionine Aminopeptidase from *Escherichia coli*: A new type of proteolytic enzyme Biochemistry 32 3907 3912
21 Spraggon, G., Schwarzenbacher, R., Kreusch, A., McMullan, D., Brinen, L. S., Canaves, J. M., Dai, X., Deacon, A. M., Elsliger, M. A., Eshagi, S., Floyd, R., Godzik, A., Grittini, C., Grzechnik, S. K., Jaroszewski, L., Karlak, C., Klock, H. E., Koesema, E., Kovarik, J. S., Kuhn, P., McPhillips, T. M., Miller, M. D., Morse, A., Moy, K., Ouyang, J., Page, R., Quijano, K., Rezezadeh, F., Robb, A., Sims, E., Stevens, R. C., van den Bedem, H., Velasquez, J., Vincent, J., von Delft, F., Wang, X., West, B., Wolf, G., Xu, Q., Hodgson, K. O., Wooley, J., Lesley, S. A., and Wilson, I. A.**2004** Proteins 56 396 400
22 Addlagatta, A., Hu, X., Liu, J. O., and Matthews, B. W.**2005** Structural basis for the finctonal differences between type I and type II human methionine aminopeptidases Biochemistry 44 14741 14749
23 D'souza, V. M., Bennett, B., Copik, A. J., and Holz, R. C.**2000** Characterization of the Divalent Metal Binding Properties of the Methionyl Aminopeptidase from *Escherichia coli* Biochemistry 39 3817 3826
24 Cosper, N. J., D'souza, V., Scott, R., and Holz, R. C.**2001** Structural Evidence that the Methionyl Aminopeptidase from *Escherichia coli* is a Mononuclear Metalloprotease Biochemistry 40 13302 13309
25 Ye, Q. Z., Xie, S. X., Ma, Z. Q., Huang, M., and Hanzlik, R. P.**2006** Structural Basis of Catalysis by Monometalated Methionine Aminopeptidase Proc. Natl. Acad. Sci. U.S.A. 103 9470 9475
26 Lowther, T. W., Zhang, Y., Sampson, P. B., Honek, J. F., and Matthews, B. W.**1999** Insights into the mechanism of *E. coli* methionine aminopeptidase from the structural analysis of reaction products and phosphorous-based transition state analogs Biochemistry 38 14810 14819
27 Huang, M., Xie, S. X., Ma, Z. Q., Hanzlik, R. P., and Ye, Q. Z.**2006** Metal mediated inhibition of methionine aminopeptidase by quinolinyl sulfonamides Biochem. Biophys. Res. Commun. 339 506 513

28 Li, J.-Y., Cui, Y.-M., Chen, L.-L., Gu, M., Li, J., Nan, F. J., and Ye, Q. Z.**2004** Mutations at the S1 Sites of Methionine Aminopeptidases from *Escherichia coli* and *Homo sapiens* Reveal the Residues Critical for Substrate Specificity J. Biol. Chem. 279 21128 21134
29 D'souza, V. M., and Holz, R. C.**1999** The Methionyl Aminopeptidase from *Escherichia coli* is an Iron(II) Containing Enzyme Biochemistry 38 11079 11085
30 D'souza, V. M., Bennett, B., and Holz, R. C.**2000** Characterization of the Divalent Metal Binding Properties of the Methionyl Aminopeptidase from *Escherichia coli* Biochemistry 39 3817 3826
31 Salomaa, P., Schaleger, L. L., and Long, F. A.**1964** Solvent Deuterium Isotope Effects on Acid-Base Equilibria J. Am. Chem. Soc. 86 1 7
32 Albery, W. J. (1975) Proton Transfer Reactions, Chapman & Hall, London.
33 Venkatasubban, K. S., and Schowen, R. L.**1984** The proton inventory technique CRC Crit. Rev. Biochem. 17 1 44
34 Elrod, J. P., Hogg, J. L., Quinn, D. M., Venkatasubban, K. S., and Schowen, R. L.**1980** Protionic reorganization and substrate structure in catalysis by serine proteases J. Am. Chem. Soc. 102 3917 3922
35 Izatt, R. M., and Christensen, J. J. (1976) Heats of proton ionization, pK, and related thermodynamic quantities, 3rd ed., Vol. 1, CRC Press, Cleveland, OH.
36 Winzor, D. J., and Sawyer, W. H. (1995) Quantitative Characterization of Ligand Binding, Wiley-Liss, New York.
37 Griffith, E. C., Su, Z., Niwayama, S., Ramsay, C. A., Chang, Y.-H., and Liu, J. O.**1998** Molecular recognition of angiogenesis inhibitors fumagillin and ovalicin by methionine aminopeptidase 2 Proc. Natl. Acad. Sci. U.S.A. 95 15183 15188
38 Larrabee, J. A., Leung, C. H., Moore, R., Thamrong.nawasawat, T., and Wessler, B. H.**2004** Magnetic Circular Dichroism and Cobalt(II) Binding Equilibrium Studies of *Escherichia coli* Methionyl Aminopeptidase J. Am. Chem. Soc. 126 12316 12324
39 Hu, X. V., Chen, X., Han, K. C., Mildvan, A. S., and Liu, J. O.**2007** Kinetic and Mutational Studies of the Number of Interacting Divalent Cations Required by Bacterial and Human Methionine Aminopeptidases Biochemistry 46 12833 12843
40 Wang, J., Sheppard, G. S., Lou, P., Kawai, M., Park, C., Egan, D. A., Schneider, A., Bouska, J., Lesniewski, R., and Henkin, J.**2003** Physiologically relevant metal cofactor for methionine aminopeptidase-2 is manganese Biochemistry 42 5035 5042
41 Chai, S. C., Wang, W.-L., and Ye, Q.-Z.**2008** Fe(II) is the native cofactor for *Escherichia coli* methionine aminopeptidase J. Biol. Chem. 283 26879 26885
42 Whiting, A. K., Boldt, Y. R., Hendrich, M. P., Wackett, L. P., and Que, L.**1996** Manganese(II)-dependent extradiol-cleaving chatechol dioxygenase from *Arthrobacter globiformis* CM-2 Biochemistry 35 160 170
43 Cleland, W. W.**1982** Use of isotope effects to elucidate enzyme mechanisms Crit. Rev. Biochem. 13 385 427
44 Kaiser, E. T., and Kaiser, B. L.**1972** Carboxypeptidase A. Mechanistic analysis Acc. Chem. Res. 5 219 224
45 Bzymek, K. P., and Holz, R. C.**2004** The Catalytic Role of Glutamate-151 in the Leucine Aminopeptidase from *Aeromonas proteolytica* J. Biol. Chem. 279 31018 31025
46 Wang, Z., Fast, W., Valentine, A. M., and Benkovic, S. J.**1999** Metallo-β-lactamase: Structure and mechanism Curr. Opin. Chem. Biol. 3 614 622
47 Chen, G., Edwards, T., D'souza, V. M., and Holz, R. C.**1997** Mechanistic studies on the aminopeptidase from *Aeromonas proteolytica*: A two-metal ion mechanism for peptide hydrolysis Biochemistry 36 4278 4286